Journal of Molecular Catalysis A: Chemical 331 (2010) 50–57

Contents lists available at ScienceDirect

Journal of Molecular Catalysis A: Chemical

journal homepage: www.elsevier.com/locate/molcata

Effect of isomorphic substitution of zirconium on mesoporous silica as support for cobalt Fischer–Tropsch synthesis catalysts

Congliang Tao[a], Jinlin Li[a,*], Yuhua Zhang[a], Kong Yong Liew[b]

[a] Key Laboratory of Catalysis and Materials Science of the State Ethnic Affairs Commission & Ministry of Education, South-central University for Nationalities, No. 708 Minyuan Road, Wuhan 430074, Hubei, China
[b] Faculty of Industrial Science and Technology, University Malaysia Pahang, Gambang 26300, Kuantan, Pahang, Malaysia

ARTICLE INFO

Article history:
Received 2 February 2010
Received in revised form 13 July 2010
Accepted 3 August 2010
Available online 11 August 2010

Keywords:
Fischer–Tropsch synthesis
Cobalt catalyst
SBA-15
Zirconium
Isomorphic substitution

ABSTRACT

Isomorphically Zr-substituted mesoporous SBA-15 with Zr/Si atomic ratios of 1/100, 1/50, 1/20, 1/8 and 1/3 have been successfully synthesized. It was demonstrated that the Zr^{4+} ions were introduced into the framework of SBA-15 with the hexagonal array of uniform tubular channel configuration intact up to a Zr/Si ratio of 1/20. Another sample of zirconium, impregnated SBA-15 to incipient wetness with a Zr/Si ratio of 1/20 was prepared for comparison. These mesoporous materials were loaded with 10 wt.% cobalt by incipient wetness impregnation and characterized by XRD, TEM, N_2 absorption–desorption, UV–visible, H_2-TPR, H_2-TPD, O_2 titration, and NH_3-TPD as well as XPS. It was shown that the introduction of zirconium produced weak acidic sites, changed the interaction between the cobalt species and the support, and improved the cobalt reducibility. The performance of catalysts for Fischer–Tropsch synthesis was tested in a fixed bed reactor, the cobalt catalyst supported on the isomorphically Zr-substituted mesoporous SBA-15 with a Zr/Si ratio of 1/20 showed the best performance.

1. Introduction

Fischer–Tropsch synthesis (FTS) is attractive for production of high-quality liquid fuels from alternative sources, such as natural gas, coal and biomass via syngas conversion over cobalt or iron based catalysts [1,2]. The cobalt based catalysts have high activity and high selectivity to linear hydrocarbons and low activity for the water gas shift (WGS) reaction [3]. The catalytic activity depends mainly on the density of surface metallic cobalt and correlated to its dispersion and reducibility which are significantly influenced by the texture and surface chemical properties of the supports [4–6].

SBA-15 is a silica-based mesoporous material with uniform hexagonal channels of 3–30 nm and has very narrow pore size distribution [7]. It is an attractive catalyst support with large surface area allowing the dispersion of a large number of catalytically active species. However, SBA-15, as a pure silica material, has low activity for some catalytic reactions, such as acid catalyzed reactions and photocatalytic reactions. Thus, incorporating SBA-15 with zirconium [8], titanium [9], aluminum [10], and vanadium [11] has attracted much attention. Newalkar et al. [8] utilized a microwave-assisted hydrothermal method to synthesize Zr-SBA-15 with different zirconium contents. The ordering of meso-structure, high surface area, and uniform pore size distribution are still maintained in the crystallized samples with a Si/Zr ratio of 20, and compared to conventional hydrothermal method, microwave-assisted hydrothermal method requires less time for aging. For FTS research, the performance of SBA-15 supported cobalt catalysts has been reported by many researchers [12–15]. However, there are few reports on incorporation of metal on SBA-15 supported cobalt catalysts for Fischer–Tropsch synthesis.

Zirconia is a transition metal oxide with acid and alkali sites as well as redox ability. As a promoter, it enhances the activity and C_{5+} selectivity for FTS reaction [16–18]. Recently, mesoporous materials, such as Zr-MCM-41 and Zr-FSM-16 [19,20], incorporating zirconium have received considerable attention in FTS catalysis because of their high surface area and porosity. As supports for cobalt catalysts, these zirconium incorporated mesoporous materials have been shown to have good catalytic performance for FTS. Liu et al. [21] reported the incorporation of zirconium in SBA-15 using various methods, including wet impregnation, coprecipitation, isomorphic substitution and grafting. One of the interesting conclusions was that the zirconium incorporated SBA-15 prepared by isomorphic substitution as support for cobalt catalysts showed higher activity than the one prepared by incipient wetness impregnation, but lower activity than that prepared by grafting at the same cobalt loading. However, the effect of zirconium content and the interaction of metallic cobalt and the support were not elucidated. In the present work, a series of Co/SBA-15 catalysts with isomorphic substituted zirconium was synthesized, and

* Corresponding author. Tel.: +86 027 67843016; fax: +86 027 67842752.
E-mail addresses: jinlinli@hotmail.com, lij@mail.scuec.edu.cn (J. Li).

1381-1169/$ – see front matter © 2010 Elsevier B.V. All rights reserved.
doi:10.1016/j.molcata.2010.08.002

another sample of Co/SBA-15 catalyst with zirconium impregnated by incipient wetness with a Zr/Si ratio of 1/20 was prepared for comparison. These materials were characterized by XRD, TEM, N_2 absorption–desorption, UV–visible, NH_3-TPD, H_2-TPR, H_2-TPD, O_2 titration as well as XPS, and their catalytic performances for FTS were tested in a fixed bed reactor. The aim is to investigate systematically the effect of different zirconium contents on the structure of the mesoporous silica supports, the activity and selectivity of the cobalt catalysts. The incorporation of zirconium in SBA-15 by the two methods (isomorphic substitution and incipient wetness impregnation) at a Zr/Si ratio of 1/20 of the supported cobalt catalysts was investigated in detail.

2. Experimental

2.1. Sample preparation

2.1.1. Materials

Tetraethyl orthosilicate (TEOS) and zirconium nitrate ($Zr(NO_3)_4{\cdot}5H_2O$) were used as silicon and zirconium sources, respectively. Triblock poly (ethylene oxide)–poly (propylene oxide)–poly (ethylene oxide) (P123, EO_{20}–PO_{70}–EO_{20}, M_{AV} = 5800, Aldrich) was used as template.

2.1.2. Supports

Zirconium isomorphic substituted mesoporous SBA-15 were prepared following the procedure reported previously [8,22] with some minor alterations: P123 (4.0 g), 2 M HCl (140 ml) and $Zr(NO_3)_4{\cdot}5H_2O$ were mixed at 35 °C to obtain a clear solution. Subsequently, TEOS (8.32 g) was gradually added to the solution with stirring for 24 h at ambient conditions. Then, the mixture (with Zr/Si atomic ratios of 1/100, 1/50, 1/20, 1/8, 1/3) was hydrothermally treated under microwave irradiation at 100 °C for 2 h by using a constant heating power of 400 W. Then the mixture was evaporated at 80 °C and finally calcined in flowing air at 550 °C for 5 h. The samples were labeled as ZS(x)-s with x standing for the Zr/Si atomic ratio.

For comparison, another sample was prepared by incipient wetness impregnation of SBA-15 using an aqueous solution containing the desired amount of zirconium nitrate with Zr/Si atomic ratio of 1/20 labeled as ZS(1/20)-i. SBA-15 and ZrO_2 were prepared following reported procedures [7,23]. The compositions of the supports are shown in Table 1.

2.1.3. Catalysts

The catalysts of 10Co/SBA-15, 10Co/ZS(x)-s, 10Co/ZS(1/20)-i and 10Co/ZrO_2 with cobalt loading (10 wt.%) were prepared by incipient wetness impregnation with the desired amount of aqueous cobalt nitrate ($Co(NO_3)_2{\cdot}6H_2O$). They were dried at 120 °C for 12 h and calcined at 450 °C in flowing air for 5 h.

Table 1
Supports composition.

Sample	Zr/Si[a]	Zr[b] (wt.%)	Zr[c] (wt.%)
SBA-15	0	0	0
ZS(1/100)-s	1/100	1.41	1.27
ZS(1/50)-s	1/50	3.12	2.68
ZS(1/20)-s	1/20	7.07	6.43
ZS(1/20)-i	1/20	7.07	6.28
ZS(1/8)-s	1/8	14.47	14.09
ZS(1/3)-s	1/3	30.31	29.39
ZrO_2	–	–	–

[a] Atomic ratio in starting mixture.
[b] Zr (wt.%) in starting mixture.
[c] Zr (wt.%) obtained by ICP measurement.

2.2. Characterization

2.2.1. ICP element analysis

The elemental composition was determined by ICP (Prodigy). The silica template was removed by boiling with 2.0 M NaOH solution at 100 °C for 6 h. The mixture was then filtered, distilled and dissolved in a 0.4 M HNO_3 solution [24].

2.2.2. XRD

X-ray powder diffraction (XRD) patterns for the calcined samples were recorded with a Bruker advanced D8 powder diffractometer (Cu Kα). The lower and wider scan ranges were 0.5–5° and 10–80° with 0.016° steps, respectively. The crystallite phase was estimated with the data of Joint Committee on Powder Diffraction Standards (JCPDS).

2.2.3. TEM

Transmission electron microscopy (TEM) characterization of the samples was carried out using an FEI Tecnai G^2-20 instrument. The samples were crushed in an agate mortar, dispersed in ethanol and dropped onto copper grids for observation.

2.2.4. Diffuse reflectance spectroscopy

Diffuse reflectance UV–visible spectra were recorded on a Hewlett-Packard 8452 A diode array spectrometer equipped with a Harrick praying mantis under ambient conditions. Wafer was made by pressing 100 mg of powder in a sample holder. The final spectra of ZS(x)-s were obtained using pure siliceous SBA-15 as the background [25].

2.2.5. N_2 absorption–desorption

N_2 absorption–desorption experiment was conducted at −193 °C using a Quantachrome Autosorb-1-C-MS instrument. Prior to the experiment, the sample was outgassed at 200 °C for 6 h. The surface area was obtained by using the BET model for adsorption data in a relative pressure ranged from 0.05 to 0.30. The total pore volumes were calculated from the amount of N_2 vapor adsorbed at a relative pressure of 0.99. The pore size distribution was evaluated from the desorption branches of the isotherms by using the Barrett–Joyner–Halenda (BJH) method.

2.2.6. NH_3-TPD

Temperature-programmed desorption of NH_3 (NH_3-TPD) was carried out in a flow apparatus. After the sample was pretreated, the sample (0.05 g) was first kept in stream of He at 100 °C for 1 h. Then, 5% NH_3/He stream (60 cm^3 min^{-1}) was flown through the sample at 100 °C for 2 h. Subsequently, the sample was flushed with He at 100 °C for 1.5 h, and the temperature was raised to 800 °C in flowing He (60 cm^3 min^{-1}) at a rate of 10 °C min^{-1}. The concentration of NH_3 in the exit gas was determined using thermal conductivity detector (TCD).

2.2.7. XPS

The surface composition of the catalysts was determined by X-ray photoelectron spectroscopy (XPS) using a Thermo VG scientific ESCA MultiLab-2000 spectrometer with a monochromatized Al Kα source (1486.6 eV) at constant analyzer pass energy of 25 eV. The binding energy was estimated to be accurate within 0.2 eV. All binding energies (BEs) were corrected referencing to the C1s (284.6 eV) peak of the contamination carbon as an internal standard. The Co 2p binding energy of the core level was determined by computer fitting of the measured spectra.

2.2.8. H_2-TPR

H_2-TPR was performed in a Zeton Altamira AMI-200 unit. Prior to the H_2-TPR measurement, the sample (0.05 g) was first flushed

with Ar (30 cm^3 min^{-1}) at 150 °C for 1 h, and then cooled down to 50 °C. Subsequently, 10% H_2/Ar (30 cm^3 min^{-1}) was flown through the catalyst while the temperature was increased to 800 °C at a rate of 10 °C min^{-1}, and was held at 800 °C for 30 min. The H_2 consumption (TCD signal) was recorded automatically by a PC.

2.2.9. H_2-TPD and O_2 titration

H_2-TPD was also performed using the Zeton Altamira AMI-200 unit. The catalyst was reduced at 450 °C for 12 h using H_2 and then cooled to 100 °C under flowing Ar to remove weakly bound physisorbed species. Then, the temperature was slowly increased to 450 °C at a ramp rate of 10 °C min^{-1}, the catalyst was held at this temperature under flowing Ar to desorb the remaining chemisorbed H_2, and the TCD signal was recorded until it returned to the baseline. The TPD spectra were integrated and the amount of desorbed H_2 was determined by comparing to the mean area of calibrated H_2 pulses.

O_2 titration was performed after reduction as described above: the catalyst was kept in flowing Ar at 450 °C and was reoxidized by injecting pulses of O_2. The flow rate was set at 30 cm^3 min^{-1}. The reducibility was calculated by assuming that metal Co was oxidized to Co_3O_4 [26].

2.3. Catalytic evaluation

Fischer–Tropsch synthesis was performed in a tubular fixed bed reactor (id = 12 mm). The catalyst (0.5 g) was mixed with 5 g carborundum and then reduced in H_2 (space velocity of 6 NL h^{-1} g^{-1}) at atmospheric pressure. The reactor temperature was increased from ambient to 100 °C (held 120 min), then, increased to 450 °C in 2 h and held for 10 h. Subsequently, the reactor was cooled down to 150 °C. Then, the syngas (CO/H_2 = 1:2, space velocity of 8 SL h^{-1} g^{-1}) was switched on and the pressure was increased to 1.0 MPa. The reactor temperature was raised to 230 °C at 1 °C min^{-1} and the reaction was carried out at 230 °C. The products were collected in a hot trap (130 °C) and a cold trap (−2 °C) in sequence. The outlet gases were analyzed online by an Agilent 3000A MicroGC, the oil (collected at −2 °C) was analyzed by an Agilent 6890N GC and the solid wax (collected at 130 °C) was analyzed by an Agilent 7890A GC.

3. Results and discussion

3.1. Characterization

3.1.1. X-ray powder diffraction

The powder XRD patterns of the supports within the range of 0.5–5° are shown in Fig. 1. When the Zr/Si atomic ratio is lower than 1/20, three well-resolved characteristic diffraction peaks at 2θ values ranging from 0.9° to 2° can be clearly observed. These are indexed to the (1 0 0), (1 1 0) and (2 0 0) reflections of the hexagonal P6mm space group, similar to the SBA-15 reported by Zhao et al. [7]. It indicates that the hexagonal structure of SBA-15 was preserved during the synthesis and subsequent calcinations of ZS(x)-s. When Zr/Si atomic ratio is higher than 1/20, the intensity of the peak near 2θ = 0.9° decreases with increasing atomic ratio and the peaks indexed to (1 1 0) and (2 0 0) diffraction disappear, while the peak indexed to (1 0 0) remains clearly observable, indicating gradual lowering of the long rang order at higher content of zirconium. When ZS(1/20)-s and ZS(1/20)-i are compared, three characteristic peaks of SBA-15 materials can be observed from the former, while for the latter, two characteristic peaks of SBA-15 materials disappear, showing that the hexagonal structure of SBA-15 was better preserved when the sample was prepared by isomorphic substitution.

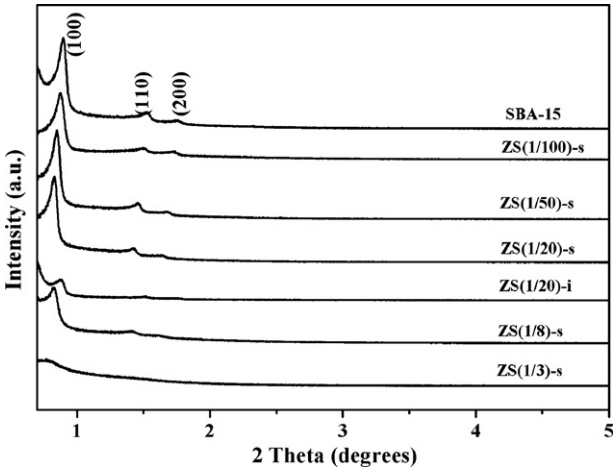

Fig. 1. Small-angle XRD patterns of the supports.

For catalysts with a Zr/Si atomic ratio lower than 1/20, the diffraction peaks at 2θ of 31.3°, 36.9°, 45.1°, 59.4° and 65.4° (Fig. 2) indicate that cobalt species were primarily in the form of spinel Co_3O_4 on the catalysts after calcinations at 450 °C. The characteristic peaks of zirconium compounds are not observed, showing that zirconium was well dispersed in the SBA-15 matrix. When the Zr/Si atomic ratio is higher than 1/20, the characteristic peaks (peak α) belonging to the tetragonal ZrO_2 phase are observed and the peak intensity of the tetragonal ZrO_2 phase increases with increasing Zr/Si ratio, showing that isolated particles of tetragonal ZrO_2 appeared on the surface of the catalysts. When ZS(1/20)-s, for sample prepared by isomorphic substitution, and ZS(1/20)-i, for sample prepared by impregnation, are compared isolated particles of tetragonal ZrO_2 phase appears in the latter, indicating that zirconium was not well dispersed in the structure of SBA-15 when the sample was prepared by impregnation.

3.1.2. Transmission electron microscopy

The transmission electron micrographs of the samples (a) ZS(1/50)-s and (b) ZS(1/8)-s are shown in Fig. 3. It can be observed that the sample ZS(1/50)-s still retains a regular hexagonal array of uniform channels, characteristic of mesoporous SBA-15 materials, while the meso-structure of sample ZS(1/8)-s is partially destroyed. Moreover, no pure ZrO_2 particle can be observed in the nanochannels by TEM-mapping.

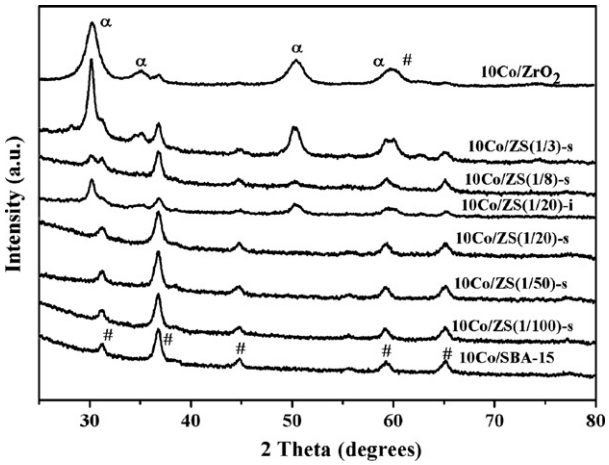

Fig. 2. Wide-angle XRD patterns of the catalysts (α: ZrO_2; #: Co_3O_4).

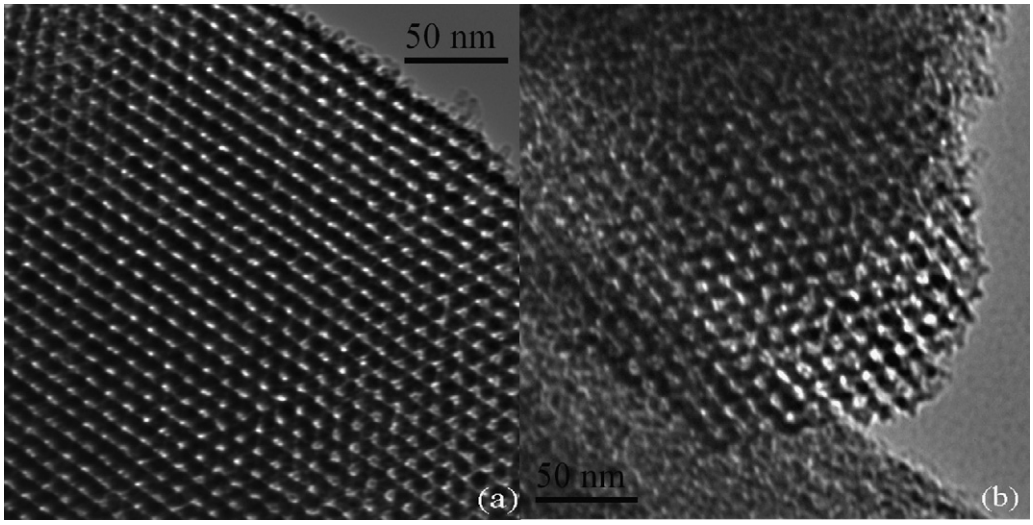

Fig. 3. TEM images of the supports: (a) ZS(1/50)-s; (b) ZS(1/8)-s.

3.1.3. Diffuse reflectance (DR) UV–vis spectroscopy

Diffuse reflectance (DR) UV–vis spectroscopy is a useful technique for studying the local coordination environment and electronic state of isolated transition metal ions or aggregated transition metal oxides [27]. It has been reported that characteristic absorption peaks in the 205–215 nm range were observed on zirconium modified mesoporous molecular sieves due to $O^{2-} \rightarrow Zr^{4+}$ of the $p \rightarrow d$ electronic transition in the framework of mesoporous molecular sieves [28,29]. Fig. 4 shows DR UV–vis spectra of the samples along with those of pure SBA-15 and ZrO_2. All of the samples containing zirconium exhibit a band around 210 nm attributable to $O^{2-} \rightarrow Zr^{4+}$ charge-transfer transition except for ZS(1/20)-i and ZS(1/3)-s. These absorption peaks are obviously different from that of the pure ZrO_2 which has a characteristic absorption peak at 230 nm, showing that the Zr^{4+} ions entered into the framework of SBA-15. The samples of ZS(1/20)-i and ZS(1/3)-s show a single band at about 230 nm, attributed to the characteristic absorption peak of the pure ZrO_2 sample, indicating that some Zr^{4+} ions isolated from the framework of the SBA-15 and the particles of tetragonal ZrO_2 phase appeared on the surface, as revealed similarly by wide-angle XRD.

3.1.4. Nitrogen adsorption–desorption

The nitrogen adsorption–desorption isotherms of the catalysts are shown in Fig. 5. For the catalysts, except 10Co/ZS(1/20)-i and 10Co/ZS(1/3)-s, the nitrogen adsorption–desorption isotherms show an obvious H1 hysteresis loop at high relative pressure, characteristic of ordered mesoporous materials, and the isotherms are similar to that of the SBA-15, indicating that the mesoporous structure did not change significantly during the synthesis and subsequent calcinations. However, for 10Co/ZS(1/20)-i and 10Co/ZS(1/3)-s, the isotherms are not very regular, suggesting that the mesoporous structure of SBA-15 was partially destroyed.

As shown in Table 2, the BET surface area (S_{BET}), pore volume (V_{BJH}) and average pore diameter (d_{BJH}) of the catalysts decrease with increasing Zr/Si atomic ratio. The BET surface area and the pore volume decrease clearly with Zr/Si atomic ratio >1/20, showing that the periodic mesoporous structure was partially collapsed during the synthesis and subsequent calcinations with a high content of zirconium. Moreover, the pore size decreases gradually with increasing Zr/Si atomic ratio, perhaps due to the formation of single ZrO_2 particle outside the meso-structure blocking the mesoporous channels. When 10Co/ZS(1/20)-s and 10Co/ZS(1/20)-i are com-

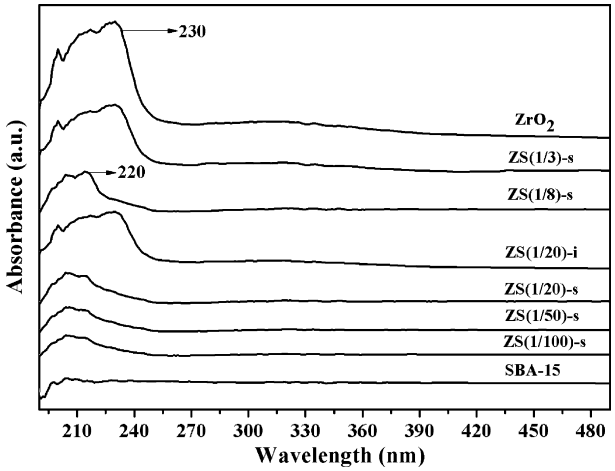

Fig. 4. Diffuse reflectance UV–vis spectra of the supports.

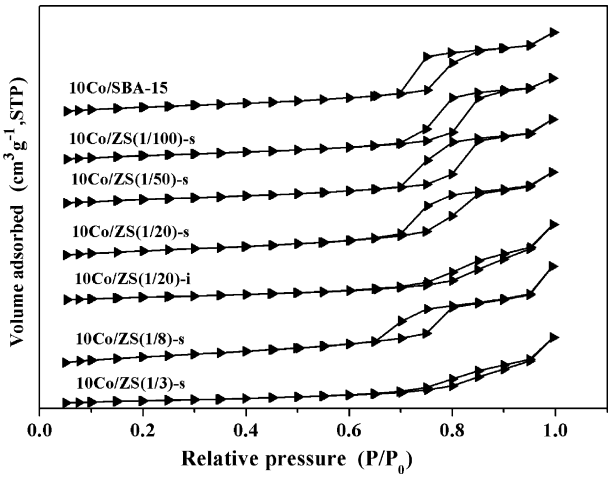

Fig. 5. N_2 absorption–desorption isotherms of the catalysts.

Table 2
N_2 physisorption results.

Sample	S_{BET} ($m^2\ g^{-1}$)	V_{BJH} ($cm^3\ g^{-1}$)	d_{BJH} (nm)
10Co/SBA-15	563.0	1.121	9.8
10CoZS(1/100)-s	515.9	1.097	8.5
10Co/ZS(1/50)-s	463.4	1.033	7.9
10Co/ZS(1/20)-s	419.9	1.028	7.7
10Co/ZS(1/20)-i	376.9	0.613	7.2
10Co/ZS(1/8)-s	291.2	0.969	6.5
10Co/ZS(1/3)-s	226.3	0.528	6.3
10Co/ZrO_2	113.2	0.256	5.8

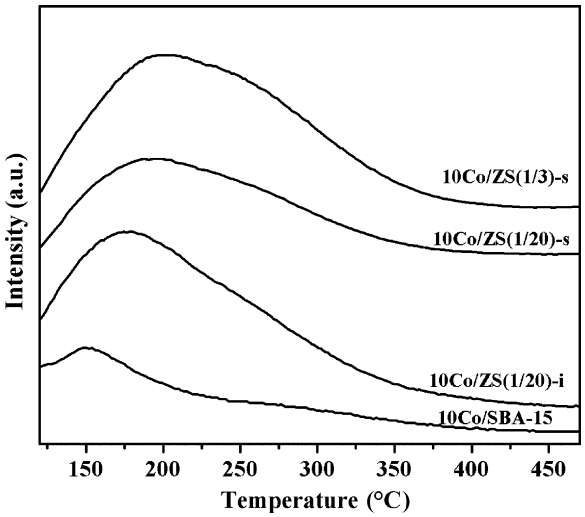

Fig. 6. NH_3-TPD profiles of the catalysts.

pared, the BET surface area, pore volume and average pore diameter of the former are larger than those of the latter, showing that the mesoporous structure of SBA-15 was better preserved when the sample was prepared by isomorphic substitution, as indicated by XRD results.

3.1.5. Ammonia temperature-programmed desorption (NH_3-TPD)

The NH_3-TPD patterns of the catalysts are shown in Fig. 6. Only one stage desorption of NH_3 is observed, the desorption peaks appearing at 150–300 °C are attributed to the weak acid sites [30]. Table 3 gives the number of acid sites expressed as m mol NH_3/g of catalysts, and the number of weak acid sites increases with increasing zirconium content. When 10Co/ZS(1/20)-s and 10Co/ZS(1/20)-i are compared the former has the larger number of acid sites, and these catalysts possess Lewis type acid sites [31].

Table 3
Surface acidity of catalysts measured by NH_3-TPD.

Sample	Acidic site (m mol NH_3/g)
10Co/SBA-15	1.36
10Co/ZS(1/20)-i	2.98
10Co/ZS(1/20)-s	3.17
10Co/ZS(1/3)-s	3.78

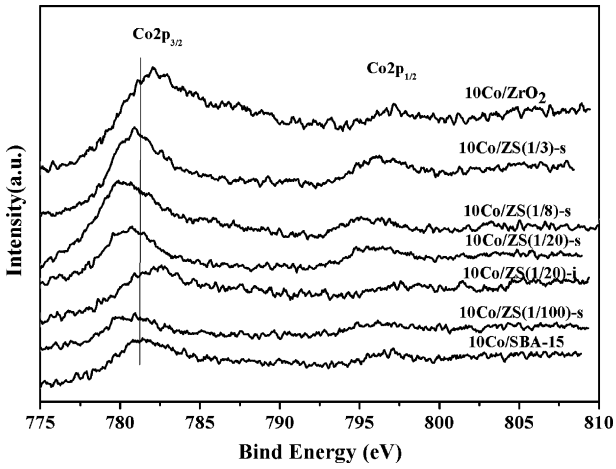

Fig. 7. XPS spectra of the Co 2p level for catalysts.

In general, a solid acid could be defined as a Lewis acid, when it shows the tendency to create dative bond due to electronic vacancies in its structure, or as a Bronsted acid, when it is able to release proton. Bosman et al. [32] found that SiO_2–ZrO_2 mixed oxides with 75 wt.% ZrO_2 or less have strong Lewis acidity. Some mixed oxides display acid property and are important catalysts in several heterogeneous reactions, such as cracking, isomerizations, Friedel–Crafts reactions, etc. [33,34]. Specifically, Lewis acid shows electronic effects which are relevant to metal–support interaction [35]. The metal–support interaction perhaps influences the cobalt reducibility (discussed in Sections 3.1.6 and 3.1.7).

3.1.6. X-ray photoelectron spectroscopy

X-ray photoelectron spectroscopy (XPS) was used to investigate the surface composition of catalysts. The XPS data are shown in Table 4 and Fig. 7. The binding energies (BEs) for Co $2p_{3/2}$ of the catalysts decrease apparently with increasing Zr/Si atomic ratio but remain in the region of 780.44 eV for 10Co/ZS-s(1/20) and 781.78 eV for 10Co/ZrO_2, This suggests that the main phase on the catalysts surface is Co_3O_4, in agreement with the XRD results. The BE of Co $2p_{3/2}$ in 10Co/SBA-15 is higher than that of pure Co_3O_4 (BE = 780.3 eV) [36], showing that the cobalt–silica phase was formed on the catalyst surface. Similar results were reported by Zhou et al. [37]. Moreover, the surface concentration of cobalt increases as detected by XPS by addition of zirconium.

An interesting feature in our XPS spectra of the Co 2p regions for catalysts is the shift to lower BE value of Co $2p_{3/2}$ by addition of zirconium, but still higher than that of pure Co_3O_4. For cobalt, the BE of Co-metal has the lowest BE for all cobalt chemical states. The binding energies of the Co $2p_{3/2}$ electrons increase from Co^0 to

Table 4
Summaries of XPS characterization of the catalysts.

Samples	Co $2p_{3/2}$ (eV)	Si $2p_{3/2}$ (eV)	Zr $3d_{3/5}$ (eV)	Concentration (at.%)			
				Si	O	Co	Zr
10Co/SBA-15	781.47	102.86	–	33.01	50.77	0.75	–
10Co/ZS(1/100)-s	781.08	102.06	182.42	28.05	51.01	1.49	0.37
10Co/ZS(1/50)-s	780.88	102.19	182.52	27.31	48.56	1.53	0.74
10Co/ZS(1/20)-s	780.44	102.05	182.77	26.99	46.45	1.62	1.34
10Co/ZS(1/20)-i	780.78	102.60	182.95	24.99	53.70	1.82	1.83
10Co/ZS(1/8)-s	780.68	102.37	182.83	25.63	46.11	1.95	1.78
10Co/ZS(1/3)-s	780.84	102.55	182.91	25.21	45.23	2.21	2.34
10Co/ZrO_2	781.78	–	183.17	–	50.65	1.86	9.96

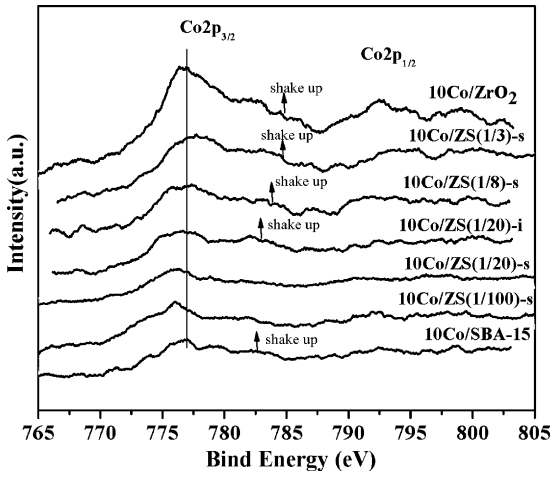

Fig. 8. XPS spectra of the Co 2p level for catalysts after reduction at 400 °C for 10 h.

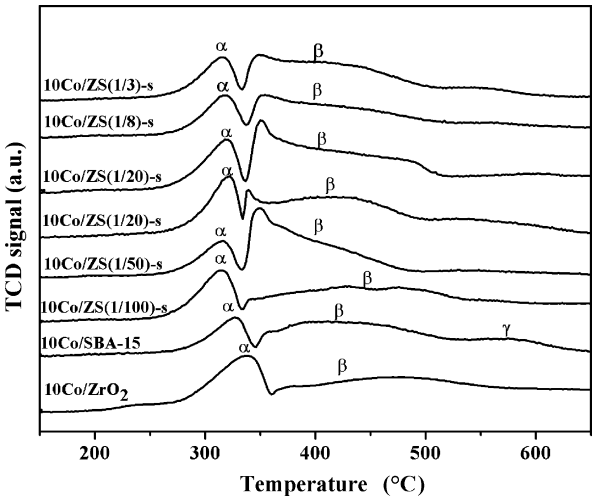

Fig. 9. H_2-TPR profiles of the catalysts.

Co^{2+} in a predictable manner. However, Co_3O_4 has a lower BE than CoO [38]. In the present study, the Co $2p_{3/2}$ matches neither with Co_3O_4 nor with CoO, and with increasing zirconium content the BE for Co $2p_{3/2}$ shifts to pure Co_3O_4, indicating that the addition of zirconium inhibited the formation of cobalt surface phase; thus, the strong interaction between the cobalt species and the support was perhaps suppressed. In the case of the catalysts with high zirconium contents (Zr/Si atomic ratio >1/20) the Co $2p_{3/2}$ peak shifts toward higher energies, implying the interaction between cobalt species and supports increases with increasing zirconium content.

The XPS spectra of catalysts reduced at 400 °C for 10 h are shown in Fig. 8. Cobalt metallic species are detected by Co $2p_{3/2}$ peak at about 777.6 eV and the Co $2p_{1/2}$ peak at about 793 eV. The oxidized Co^{2+} species were identified by XPS peaks at about 781 and 798 eV [39,40]. After reduction, a shoulder remained at the oxidic position showing that a fraction of the Co^{2+} oxide remains on the surface, and is difficult to reduce, as was observed in a study of cobalt kieselguhr Fischer–Tropsch catalysts [41]. With increasing zirconium content, the position of Co $2p_{3/2}$ shifted to lower binding energies (Zr/Si atomic ratio <1/20), and at higher zirconium content (Zr/Si atomic ratio >1/20), the Co $2p_{3/2}$ peak shifts toward higher energies, with the appearance of a high intensity shake-up satellite peaks. These features indicate the presence of Co^{2+} species in the amorphous cobalt silicate which could be taken as evidence of the strong interaction of the cobalt species [39] with the surface of the ZS(x) support at high zirconium contents.

3.1.7. Hydrogen temperature-programmed reduction (H_2-TPR)

TPR profiles of the catalysts with different Zr/Si atomic ratios are shown in Fig. 9. For 10Co/SBA-15, three reduction peaks are observed: the peak α corresponds to the first reduction step of Co_3O_4 ($Co_3O_4 \rightarrow CoO$), the peak β is attributed to the reduction of intermediate CoO phase ($CoO \rightarrow Co^0$) and the high temperature reduction peak γ is attributed to reduction of the barely reducible cobalt silicates (Co_2SiO_4) formed by the strong interaction between cobalt and the siliceous support [12]. For 10Co/ZS(x)-s, 10Co/ZS(1/20)-i and 10Co/ZrO_2, only two peaks are identified for the reduction of Co_3O_4 to CoO (peak α) and CoO to Co (peak β), and the third peak (peak γ) could barely be identified.

It is observed that by addition of zirconium, the peak position of the first reduction of Co_3O_4 is significantly shifted to lower temperature, meaning that Co_3O_4 particles supported on ZS(x)-s or ZS(x)-i are more easily reduced to CoO species, most likely due to the weakening of cobalt–silica support interaction by the addition of zirconium, as revealed by XPS; similar findings was reported by Moradi et al. [18]. The peak position of the second reduction is not shifted significantly. In the supported catalysts, the reducibility of cobalt species often depends on the extent of the metal–support interaction. By addition of zirconium at lower content, the cobalt–silica support interaction decreases, improving the reduction of CoO to Co, while at higher zirconium content, perhaps the increased concentration of cobalt species and interaction with the surface decreased the reduction of CoO to Co, as shown in the XPS results. For 10Co/ZS(1/20)-s, the peak area of the second reduction appears to be larger than that of 10Co/ZS(1/20)-i, suggesting that incorporation of zirconium with isomorphic substitution was superior in improving the degree of reduction of the catalysts.

Table 5
H_2-TPD and O_2 titration data.

Sample	H_2 desorbed (μmol/g)	D_{uncor}[a] (%)	d_{uncor}[b] (nm)	O_2 uptaked (μmol/g)	Red (%)	D_{corr}[c] (%)	d_{corr}[d] (nm)
10Co/SBA-15	66.2	7.19	19.1	306.2	22.05	32.61	4.2
10Co/ZS(1/100)-s	61.0	6.74	22.3	637.4	46.32	14.55	10.3
10Co/ZS(1/50)-s	57.2	6.01	21.7	783.0	52.89	11.36	11.5
10Co/ZS(1/20)-s	54.9	5.82	22.7	888.7	58.17	10.01	13.2
10Co/ZS(1/20)-i	48.6	4.52	36.2	678.3	48.02	9.41	17.4
10Co/ZS(1/8)-s	41.3	3.46	43.6	551.8	43.71	7.92	19.1
10Co/ZS(1/3)-s	38.6	2.61	58.7	491.2	37.48	6.96	22.0
10Co/ZrO_2	32.2	1.91	64.1	364.7	28.33	6.74	18.2

[a] Uncorrected catalyst dispersion.
[b] Uncorrected metal cluster diameter.
[c] Corrected catalyst dispersion.
[d] Corrected metal cluster diameter.

Table 6
Performances of the catalysts in a fixed bed reactor.[a]

Catalysts	X_{CO} (%)	Products selectivity (mol%)				
		Methane	Olefin[b]	n-Paraffin	Isomer[c]	C_{5+} hydrocarbon
10Co/SBA-15	15.47	18.07	9.16	67.21	4.08	71.28
10Co/ZS(1/100)-s	17.62	12.01	8.57	68.07	8.87	79.01
10Co/ZS(1/50)-s	25.44	8.51	7.32	68.97	13.85	83.86
10Co/ZS(1/20)-s	26.21	7.45	6.68	68.56	14.84	86.71
10Co/ZS(1/20)-i	20.97	14.37	8.08	67.42	9.13	76.86
10Co/ZS(1/8)-s	19.48	8.69	5.74	67.97	15.83	79.91
10Co/ZS(1/3)-s	18.48	13.03	4.11	66.19	16.03	82.62
10Co/ZrO_2	8.92	7.07	8.76	71.98	9.98	78.31

[a] Reaction conditions: 1.0 MPa, 230 °C, CO/H_2 = 1:2, space velocity of syngas 8 SL g^{-1} h^{-1}.
[b] Included cis-olefins, trans-olefins and 1-olefins.
[c] Included paraffin isomers.

3.1.8. Hydrogen temperature-programmed desorption (H_2-TPD) and O_2 titration

The results of H_2-TPD and O_2 titration are shown in Table 5. The uncorrected dispersions are based on the assumption of complete reduction of cobalt oxide, and the corrected dispersions are revised by percentage reduction. Without including the percentage of reduction in the calculation, the percentage dispersion is underestimated. [26], and the uncorrected metal cluster diameter is needed to be corrected by percentage reduction. As can be seen, H_2 chemisorption decreases significantly with increasing zirconium content. It indicates that the cobalt active sites decreased by addition of zirconium. The percentage reduction increases for catalysts with low zirconium contents and decreases for those with high zirconium contents. It is concluded that small amounts of zirconium suppressed the interaction between cobalt and support, and improved the reducibility of the catalysts and at high zirconium contents, the reducibility of the catalysts decreases due to the strong interaction of the cobalt species with the surface of the supports. This result was also revealed by XPS and H_2-TPR experiments. The dispersion of cobalt decreases due to the decrease of surface area and pore volume by the addition of zirconium. Meanwhile, the metal cluster size increases.

3.2. Fischer–Tropsch synthesis

3.2.1. Catalytic activity

The results of FTS activity and product selectivity of the catalysts are summarized in Table 6. The following trends are apparent: (1) With increasing zirconium content, the CO conversion increases initially on increasing zirconium from 1/100 to 1/20, but decreases with further increase in the Zr/Si ratio from 1/20 to 1/3; (2) With the same content of zirconium, the CO conversion of the 10Co/ZS(1/20)-s prepared by isomorphic substitution is higher than that of 10Co/ZS(1/20)-i prepared by co-impregnation; (3) The CO conversion of 10Co/ZrO_2 is lower than that of other catalysts under the same conditions.

It has been demonstrated that the catalytic activity of Co catalysts for FTS depended on the catalyst reducibility. In principle, the activity of reduced cobalt catalysts should be relevant to the concentration of surface metal cobalt sites [4–6,42]. For 10Co/ZS(*x*)-s, when Zr^{4+} ions were introduced into the SBA-15 framework with the hexagonal array of uniform tubular channel configuration intact, retaining high surface area and large pore volume, the probability of Zr^{4+} ions contacting Co_3O_4 particles was high. Further, with increasing zirconium content, the density of surface cobalt and the degree of reduction of Co increase, more accessible cobalt active surface sites were generated, and thus, the CO conversion increased. However, on further increasing Zr/Si atomic ratio from 1/8 to 1/3, the hexagonal array of uniform tubular channel configuration was destroyed gradually, leading to the decrease in surface area and pore volume as well as the formation of strong interaction of the cobalt species with the supports hence a decrease in the degree of reduction of cobalt. Thus, CO conversion is decreased.

The low activity of 10Co/SBA-15 can be attributed to the low reducibility of cobalt species in the catalysts. Cobalt silicates are present in the former, as discussed in H_2-TPR results. The low activity of 10Co/ZrO_2 is related to its low surface area and low pore volume. At the same content of zirconium, 10Co/ZS(1/20)-s shows higher activity compared to 10Co/ZS(1/20)-i, perhaps due to higher reducibility of cobalt species in the catalysts.

3.2.2. Product selectivity

As observed in Table 6, 10Co/SBA-15 gives the highest methane selectivity and the lowest C_{5+} hydrocarbons selectivity. For 10Co/ZS(*x*)-s, by the addition of zirconium, C_{5+} hydrocarbons selectivity increases from 79.01% to 86.71%, and then declines to 79.91%, and isomers selectivity increases from 4.08% to 16.03%, while olefin selectivity decreases from 9.16% to 4.11%. When 10Co/ZS(1/20)-s and 10Co/ZS(1/20)-i are compared, the former shows higher C_{5+} hydrocarbons and hydrocarbon isomers selectivity, lower methane and selectivity olefin.

The high methane selectivity was usually reported for catalysts having high metal dispersion and low cobalt reducibility [4,12]. This resulted in the formation of unreduced cobalt oxides which catalyzed WGS reaction. As evidenced by O_2 titration, the high cobalt dispersion and the low catalyst reducibility of 10Co/SBA-15 led to high methane selectivity. It has been demonstrated that the presence of larger cobalt particles led to higher selectivity to heavier hydrocarbons [12,43,44]. As shown in Tables 5 and 6, it is obvious that the change in the C_{5+} selectivity corresponds to the size of cobalt clusters.

Zhang et al. [45] have reported that the adjustment of surface acidity resulted in changing the interaction between the cobalt species and supports, improving the reducibility, which enhances the activity and the selectivity for heavy hydrocarbon. In the present work, the number of weak acid sites increased with increasing zirconium content (Fig. 6). On the surface of catalysts, when Zr/Si atomic ratio is <1/20, the increase in the number of acid sites may induce the change of surface charge, resulting in a decrease in the interaction between cobalt and support, increasing the reducibility of cobalt species, enhancing the activity and the selectivity for heavy hydrocarbons. At Zr/Si atomic ratio >1/20, the increased number of acid sites induces the strong interaction between cobalt and support, decreases the reducibility of cobalt species leading to the decreased activity.

The number of acid sites measured by NH_3-TPD increased in the order of 10Co/SBA-15, 10Co/ZS(1/20)-i, 10Co/ZS(1/20)-s, 10Co/ZS(1/3), and the decreased olefin selectivity and the increased hydrocarbon isomer selectivity are in the same order. The acidic catalysts promote the formation of hydrocarbon isomers at the

expense of olefins, thus reducing the olefin selectivity. Meanwhile, the hydrocarbon isomers may have been formed from linear hydrocarbons by secondary reactions such as cracking and isomerization over acidic sites. Similar conclusions have been reported by Koh et al. [46]. However, as no detailed analysis of the branched hydrocarbons was done, it is not possible to distinguish the two mechanisms.

4. Conclusions

Zirconium isomorphic substitution of SBA-15 did not affect the tubular structure of the parent SBA-15 at lower zirconium contents until a Zr/Si ratio of 1/20 but resulted in partial collapse of the mesostructure at higher extent of substitution.

By addition of zirconium, the reduction of Co_3O_4 to CoO was facilitated. At higher zirconium contents, the surface area and pore volume decreased, and the strong interaction between cobalt and supports led to the decreased reduction of CoO to Co. Further, the formation of acid sites influenced the interaction between the cobalt species and the support, hence, the reducibility of cobalt species. Consequently the catalytic performance and products selectivity of the catalysts were affected.

Compared to incipient wetness impregnation, the isomorphic substitution was superior in retaining the integrity of SBA-15 structure, improved the cobalt reducibility and showed better catalytic performance.

Acknowledgement

Financial support from National Natural Science Foundation of China (Grant Nos. 20590360 and 20773166) is gratefully acknowledged.

References

[1] B.H. Davis, Top. Catal. 32 (2005) 143–168.
[2] A.Y. Khodakov, W. Chu, P. Fongarland, Chem. Rev. 107 (2007) 1692–1744.
[3] E. Iglesia, Appl. Catal. A 161 (1997) 59–78.
[4] R.C. Reuel, C.H. Bartholomew, J. Catal. 85 (1984) 63–77.
[5] A. Barbier, A. Tuel, I. Arcon, A. Kodre, G.A. Martin, J. Catal. 200 (2001) 106–116.
[6] E. Iglesia, S.L. Soled, R.A. Fiato, J. Catal. 137 (1992) 212–224.
[7] D.Y. Zhao, J. Feng, Q. Huo, M. Melosh, G.H. Fredrickson, B.F. Chmelka, G.D. Stucky, Science 279 (1998) 548–552.
[8] B.L. Newalkar, J. Olanrewaju, S. Komarneni, J. Phys. Chem. B 105 (2001) 8356–8360.
[9] E. Sacaliuc, A.M. Beale, B.M. Weckhuysen, T.A. Nijhuis, J. Catal. 248 (2007) 235–248.
[10] T. Klimova, J. Reyesa, O. Gutiérreza, L. Lizama, Appl. Catal. A 335 (2008) 159–171.
[11] G. Dua, S. Lima, M. Pinaulta, C. Wanga, F. Fanga, L. Pfefferlea, G.L. Haller, J. Catal. 253 (2008) 74–90.
[12] A. Martínez, C. López, F. Márquez, I. Díaz, J. Catal. 220 (2003) 486–499.
[13] H.F. Xiong, Y.H. Zhang, K.Y. Liew, J.L. Li, J. Mol. Catal. A 295 (2008) 68–76.
[14] A.Y. Khodakov, R. Bechara, A. Griboval-Constant, Appl. Catal. A 254 (2003) 273–288.
[15] Y. Wang, M. Noguchi, Y. Takahashi, Y. Ohtsuka, Catal. Today 68 (2001) 3–9.
[16] S. Ali, B. Chen Jr., J.G. Goodwin, J. Catal. 157 (1995) 35–41.
[17] A. Feller, M. Claeys, E. van Steen, J. Catal. 185 (1999) 120–130.
[18] G.R. Moradi, M.M. Basir, A. Taeb, A. Kiennemann, Catal. Commun. 4 (2003) 27–32.
[19] M.D. Wei, K. Okabe, H. Arakawa, Y. Teraoka, Catal. Commun. 5 (2004) 597–603.
[20] Y.Y. Liu, T. Hanaoka, K. Murata, K. Okabe, I. Takahara, K. Sakanishi, React. Kinet. Catal. Lett. 92 (2007) 147–154.
[21] Y.Y. Liu, K. Murata, K. Okabe, T. Hanaoka, K. Sakanishi, Chem. Lett. 37 (2008) 984–985.
[22] K. Szczodrowski, B. Prelot, S. Lantenois, J. Zajac, M. Lindheimer, D. Jones, A. Julbe, A. Lee, Micropor. Mesopor. Mater. 110 (2008) 111–118.
[23] G.K. Chuah, S. Jaenieke, S.A. Cheong, K.S. Chan, Appl Catal. A 145 (1996) 267–284.
[24] Z. Lou, R. Wang, H. Sun, Y. Chen, Y. Yang, Micropor. Mesopor. Mater. 110 (2008) 347–354.
[25] Y.H. Yang, S. Lim, G.A. Du, Y. Chen, D. Ciuparu, G.L. Haller, J. Phys. Chem. B 109 (2005) 13237–13246.
[26] D.C. Song, J.L. Li, J. Mol. Catal. A 247 (2006) 206–212.
[27] S. Bordiga, R. Buzzoni, F. Geobaldo, C. Lamberti, E. Giamello, A. Zecchina, G. Leofanti, G. Petrini, G. Tozzola, G. Vlaic, J. Catal. 158 (1996) 486–501.
[28] K. Chaudhari, R. Bal, T.Kr. Das, A. Chandwadkar, D. Srinivas, S. Sivasanker, J. Phys. Chem. B 104 (2000) 11066–11074.
[29] M.S. Morey, G.D. Stucky, J. Phys. Chem. B 103 (1999) 2037–2041.
[30] F. Lónyi, J. Valyon, Micropor. Mesopor. Mater. 47 (2001) 293–301.
[31] A. Gervasini, C. Messi, D. Flahaut, C. Guimon, Appl. Catal. A 367 (2009) 113–121.
[32] H.J.M. Bosman, A.P. Pijpers, A.W.M.A. Jaspers, J. Catal. 161 (1996) 551–559.
[33] G. Sartori, R. Maggi, Chem. Rev. 106 (2006) 1077–1104.
[34] Y. Sun, S. Walspurger, J.-P. Tessonnier, B. Louis, J. Sommer, Appl. Catal. A: Gen. 300 (2006) 1–7.
[35] A. Gervasini, C. Messi, A. Ponti, S. Cenedese, N. Ravasio, J. Phys. Chem. C 112 (2008) 4635–4642.
[36] T.L. Barr, J. Vac. Sci. Technol. A 9 (1991) 1793–1805.
[37] W. Zhou, K.G. Fang, J.K. Chen, Y.H. Sun, Fuel Process. Technol. 87 (2006) 609–616.
[38] V.I. Nefedov, M.N. Firsov, I.S. Shaplygin, J. Electron Spectrosc. Relat. Phenom. 26 (1982) 65–78.
[39] S.W. Ho, M. Horialla, D.M. Hercules, J. Phys. Chem. 94 (1990) 6396–6399.
[40] D.G. Castner, P.R. Watson, I.Y. Chan, J. Phys. Chem. 94 (1990) 819–828.
[41] B.A. Sexton, A.E. Hughes, T.W. Turney, J. Catal. 97 (1986) 390–406.
[42] A.R. Belambe, R. Oukaci, J.G. Goodwin Jr., J. Catal. 166 (1997) 8–15.
[43] J. Panpranot, J.G. Goodwin Jr., A. Sayari, Catal. Today 77 (2002) 269–284.
[44] R. Trujillano, F. Villain, C. Louis, J. Lambert, J. Phys. Chem. C 111 (2007) 7152–7164.
[45] J.L. Zhang, J.G. Chen, J. Ren, Y. Sun, Appl. Catal. A: Gen. 243 (2003) 121–133.
[46] D.J. Koh, J.S. Chung, Y.G. Kim, Ind. Eng. Chem. Res. 34 (1995) 1969–1975.